Hindawi Publishing Corporation
Physics Research International
Volume 2014, Article ID 782357, 11 pages
http://dx.doi.org/10.1155/2014/782357

Research Article

Structural and Optical Investigations of Heterostructures Based on $Al_xGa_{1-x}As_yP_{1-y}$:Si Solid Solutions Obtained by MOCVD

P. V. Seredin

Joint Physics Laboratory of Nano-Heterostructures and Semiconductor Materials, Voronezh State University, Universitetskaya Square 1, Voronezh 394006, Russia

Correspondence should be addressed to P. V. Seredin; paul@phys.vsu.ru

Received 14 May 2014; Revised 4 July 2014; Accepted 8 July 2014; Published 23 July 2014

Academic Editor: Zhiqiang Mao

We investigated MOCVD epitaxial heterostructures based on $Al_xGa_{1-x}As$ ternary solid solutions, obtained in the range of compositions $x \sim 0.20$–0.50 and doped with high concentrations of phosphorus and silicon atoms. Using the methods of high-resolution X-ray diffraction, scanning electron microscopy, X-ray microanalysis, Raman spectroscopy, and photoluminescence spectroscopy we have shown that grown epitaxial films represent five-component $(Al_xGa_{1-x}As_{1-y}P_y)_{1-z}Si_z$ solid solutions. The implementation of silicon in solid solution with a concentration of ~ 0.01 at.% leads to the formation of the structure with deep levels, DX centers, the occurrence of which fundamentally affects the energy characteristics of received materials.

1. Introduction

Semiconductor solid solutions based on $A_{III}B_V$ compounds provide clear benefits compared with silicon electronics due to a number of properties as follows: the ability to control the width of the band gap by changing the composition, direct band gap, high electron mobility, and so forth. In addition, the devices based on $A_{III}B_V$ generate less noise than the same silicon devices. Because of the higher breakdown voltage devices based on $A_{III}B_V$ can operate at a higher capacity. All this opens broad range of applications and the effective use of these compounds, from electronics to photovoltaic devices and most forms of optoelectronic components including diodes and solid-state lasers.

The most demanded material for the quantum-well structures is $Al_xGa_{1-x}As$ solid solutions, with sufficiently close lattice parameters to GaAs, which is used as a substrate; thus $Al_xGa_{1-x}As$/GaAs heteropairs possess a minimum density of mismatch dislocations near the heterojunction. Doping $Al_xGa_{1-x}As$ solid solution with impurity atoms makes it easy to control the type of conductivity and electrical resistance in the heterostructure and allows one to create heterojunctions with various band gaps on the borders.

However, $Al_xGa_{1-x}As$ epitaxial layers have several disadvantages, which include high reaction abilities and reactivity of aluminum atoms with oxygen, which rises with an increasing concentration of aluminum atoms in the metal sublattice. In addition, $x \sim 0.30$ compositions correspond to a high density of deep levels and surface states. Another very important fact is that the complete match in crystal lattices parameters is impossible in $Al_xGa_{1-x}As$ /GaAs heterostructure, as the size of aluminum atoms is bigger than that of gallium and arsenic atoms. Therefore, at high x concentrations of aluminum in metal sublattice, even in such a well-coordinated heteropair, there are internal stresses which can lead to undesirable effects.

Competitive to the $Al_xGa_{1-x}As$ solid solutions for design and manufacture of optoelectronic components on GaAs there are some other ternary solid solutions based on $A_{III}B_V$, such as $Ga_xIn_{1-x}P$, $In_xGa_{1-x}As$, $Al_xGa_{1-x}P$, and quaternary $Ga_xIn_{1-x}As_yP_{1-y}$ solid solutions [1, 2]. Their fundamental structural properties (type of crystal lattice, Vegard's law, Kufala equation: the dependence of the band gap on the composition, etc.) are similar to $Al_xGa_{1-x}As$ solid solutions. However, the presence of incoherence areas of solid solutions and substrate lattice parameters, immiscibility regions [3],

Table 1: Composition and growth condition of $Al_xGa_{1-x}As_yP_{1-y}$:Si heterostructures.

Sample	Composition, x, y	T	Flow SiH_4 cm^3/min	Carrier concentration, cm^{-3}	As/P
EM2350	GaAs	800	—	3.6×10^{16}	—
EM2346	x~0.30	800	—	3.1×10^{16}	—
EM2438	x~0.25	700	10	3.4×10^{17}	—
EM2449	x~0.25	800	100	6.5×10^{17}	—
EM2342	x~0.40, y~0.98-0.99	800	100	7.85×10^{17}	30
EM2343	x~0.40, y~0.98-0.99	800	200	8.19×10^{17}	30
EM2355	x~0.50, y~0.98-0.99	800	200	7.07×10^{17}	30
EM2356	x~0.50, y~0.98-0.99	800	300	4.56×10^{17}	30

and instability (mostly refers to $Ga_xIn_{1-x}As_yP_{1-y}$) significantly limits the range of compounds that can be used to create heterostructures based on the above mentioned systems and do not always allow one to observe quantum effects.

Another viable alternative to $Al_xGa_{1-x}As$ system can be $Al_xGa_{1-x}As_{1-y}P_y$ solid solutions. Today it was shown that the implementation of low concentrations of phosphorus in the layers of $Al_xGa_{1-x}As$ heterostructure allows one to receive a minimum of internal stresses in crystal lattices and provides better heat dissipation at high pump currents and, consequently, increases the power output of the laser diode based on $Al_xGa_{1-x}As_{1-y}P_y$ [4, 5]. An increase of phosphorus in the layers of solid solution should slow down the oxidation of the surface and increase activation energy of oxidation [6]. In addition, as we have shown in previous publications, doping of $Al_xGa_{1-x}As$ solid solution with high concentrations of silicon leads to the formation of quaternary solid solutions $(Al_xGa_{1-x}As)_{1-y}Si_y$ and allows one not only to control a number of electrooptical and electrical properties, but also to coordinate lattice parameters of heteropairs by substitution of the main atoms of the solid solution by small-sized atoms. In this case, silicon embeds in $Al_xGa_{1-x}As$ solid solutions in the form of deep donor, known as DX-center with special properties. At deep levels, DX-centers can accumulate a charge capable of changing a potential profile of a heterostructure. Consequently, the conductivity of the heterostructure is determined due to the effects related to the recharging process of deep levels, as well as residual effects of a positive and negative photoconductivity [7]. All of this makes such solid solutions highly promising materials for optical converters, heterojunction, and detectors.

Thus, doping of $Al_xGa_{1-x}As$ solid solution by smaller impurity atoms, silicon and phosphorus, should allow one not only to achieve two objectives: the controlled management of a number of electrooptical and electrical properties, but also to coordinate lattice parameters of heteropairs by the substitution of the main atoms of the solid solution by small-sized atoms.

It should be noted that the progress in technology of the epitaxial growth of heterostructures on the basis of ternary or even quaternary alloys, for example, the $Ga_xIn_{1-x}As_yP_{1-y}$ alloys, is already rather considerable, and a large number of publications devoted to the unique and interesting properties of these compounds are currently available. In contrast, studies of heterostructures based on quinary alloys are few and far between. At the same time, a quinary system of alloys has an extra degree of freedom, as compared to quaternary and ternary structures [8, 9]. In turn, this allows one to produce structures with more appropriable characteristics. It becomes possible not only to vary the band gap within the range of direct gap compositions, but, for a fairly wide range of compositions, to match the constituent layers in the lattice period and thermal expansion coefficient as well.

Therefore the purpose of our research work became the investigation of structural and optical properties of multi-component solid solutions based on $Al_xGa_{1-x}As$, doped with high level concentration of phosphorus and silicon.

2. Objects and Research Methods

Epitaxial heterostructures based on $Al_xGa_{1-x}As_{1-y}P_y$ solid solutions with a thickness of ~2 μm were grown using MOCVD method on EMCORE GS 3/100 installation in a vertical reactor with a high-speed substrate holder rotation. As sources, we used trimethylgallium ($Ga(CH_3)_3$), trimethylaluminum $Al(CH_3)_3$, arsine (AsH_3), and phosphine (PH_3). We used monosilane (SiH_4) as doping components to obtain n-type conductivity. Hydrogen was used as the carrier gas. The structures were grown on n-GaAs (100) substrates.

Processing characteristics of the samples are shown in Table 1. Table 1 also shows the flow of the dopant in reactor, which consists of 0.05% of a mixture of silane in hydrogen. The carrier concentration was determined by the Hall effect at room temperature. The estimated value of the phosphorus content in the solid solution was 1-2%. Phosphorus was implemented into a layer in order to compensate for the expected bulk stresses which are caused by slightly mismatched lattice parameter, but with a significant thickness (2 μm) of $Al_xGa_{1-x}As$ layers.

The structural quality of heterostructures and determination of lattice parameters of solid solutions were determined by X-ray diffractometer Seifert HR 3003 with four circuitous goniometer and monochromatized copper radiation with a wavelength of $CuK\alpha_1$ = 1.5405 Å. The concentration of

Table 2: Energy-dispersive X-ray analysis data.

Sample	Composition of epitaxial film, at.%				
	n_{Al} at.%	n_{Ga} at.%	n_{As} at.%	n_{P} at.%	$n_{Si.}$ at.%
EM2350					
T = 800; flow = 0; carrier = 3.6×10^{16}	—	50.00	50.00	—	—
EM2346					
T = 800; flow = 0; carrier = 3.1×10^{16}	12.22	37.19	50.59	—	—
EM2438					
T = 700; flow = 10; carrier = 3.4×10^{17}	11.65	32.16	56.18	—	—
EM2449					
T = 800; flow = 100; carrier = 6.5×10^{17}	10.07	39.04	50.90	—	0.02
EM2342					
T = 800; flow = 100; carrier = 7.85×10^{17}	16.37	32.92	50.18	0.53	0.05
EM2343					
T = 800; flow = 200; carrier = 8.19×10^{17}	16.37	33.06	50.00	0.53	0.04
EM2355					
T = 800; flow = 200; carrier = 7.07×10^{17}	21.40	27.91	49.90	0.78	0.07
EM2356					
T = 800; flow = 300; carrier = 4.56×10^{17}	21.02	28.05	50.27	0.66	0.09

elements in solid solution has been refined by X-ray microanalysis using the attachment to an electron microscope. Raman spectra were obtained with a Raman microscope Renishaw 1000 with ×50 NPlan lens and the excitation by an argon laser with a wavelength of 514.5 nm. The laser beam did not exceed 3 mW. Photoluminescence spectra of heterostructures were obtained at room temperature from the sample surface by standard method with the use of monochromator TRIAX550 and cooled with liquid nitrogen CCD detector. Excitation photoluminescence spectra were produced by argon laser with a wavelength of 514.5 nm. In order to focus on the surface, ×10 lens were used.

3. Results and Discussion

At the first stage of the research using the X-ray microanalysis attachment to the electron microscope, we clarified the concentration of the elements included in solid solutions compositions. We used 20 kV electron accelerating voltage and analyzed sample area 750 × 750 μm. Effective depth for microanalysis was ~1–1.5 μm. X-ray microanalysis data is presented in Table 2. As can be seen from these results, the concentrations of atoms in solid solution are different from those specified at the growth stage. The composition of the solid solution was specified on the basis of the ratio of concentrations of the elements in the gas phase using the composition and rate of growth data for standard $Al_xGa_{1-x}As$ ternary solid solutions. However, the coefficients of segregation of elements included in solid solution may vary according to the overall composition of the gas phase, which, respectively, can lead to uncertainty in determination of composition of epitaxial layer. We note that according to the data (see Table 2) concentration of phosphorus and silicon atoms in epitaxial layer reach several parts of atomic percent. Also attention should be paid to the fact that the total concentration of atoms in the metal sublattice of five-component layers is less than in the nonmetallic sublattice.

This is most likely to be a consequence of the amphoteric behavior of silicon atoms as impurities. Looking back on the experience of the previous studies of growth processes when $Al_xGa_{1-x}As$ solid solutions were highly doped with silicon [10, 11], it is clear to see that this circumstances are sufficient for the formation of system $Al_xGa_{1-x}As_{1-y}P_y$-Si solid solutions.

To confirm our assumptions, we used high-resolution X-ray diffraction and further calculations of lattice parameters for the obtained solid solutions. Therefore, we performed the study of the structure and characteristics of grown epitaxial layers using a map of the q-space, since it allows one to receive direct information about the mismatch of lattice parameters in the epitaxial layer and substrate, disorientation or relaxation in the layer, dislocation density, its mosaic, or curvature. For each sample we produced maps of the distribution of diffracted light intensity in space around the q-symmetric (400) node and asymmetric (511) node, shown in Figures 1(a)–1(j).

The analysis of the reciprocal space maps (Figure 1) leads to the conclusion that epitaxial solid solution growth is coherent on GaAs (100) substrates, and samples have a small stress and composition gradient in the epitaxial layers, which is evidenced by the position and shape of nodes in reciprocal space for symmetric and asymmetric reflections.

Lattice parameters in directions $a^{\perp}$ and in the plane of growth $a^{\parallel}$ can be easily identified using the data obtained from the analysis of reciprocal q-space map for the symmetric (400) and asymmetric (511) reflections, as follows: $a^{\perp}$ can be determined using the information of a symmetric (400) reflection $b_{400}^{\text{epilayer}} = (4^2/a^{\perp 2})^{1/2}$ or asymmetric $b_{500}^{\text{epilayer}} = (5^2/a^{\parallel 2})^{1/2}$, while $a^{\parallel}$ is given by the following relation, considering data of the asymmetric (511) reflection: $b_{011}^{\text{epilayer}} = ((1^2 + 1^2)/a^{\parallel 2})^{1/2}$. Here, b node coordinates in reciprocal q-space.

Lattice constant of solid solutions a^{ν} with cubic symmetry taking into account the elastic stresses in heteroepitaxial layer in accordance with the linear theory of elasticity can be calculated as follows [12]:

$$a^{\nu} = a^{\perp}\frac{1-\nu}{1+\nu} + a^{\parallel}\frac{2\nu}{1+\nu}, \tag{1}$$

where ν is Poisson's coefficients for epitaxial layers.

Keeping in mind that studied samples of heterostructures were obtained with isoperiodic to GaAs compositions, we assume that the dependence of the various parameters for solid solutions will be linear. Using linear interpolation similar to which we have used in our previous work [13, 14], we can write the law of Vegard for solid solutions $(Al_xGa_{1-x}As_{1-y}P_y)_{1-z}Si_z$ first through ternary and then through the binary compounds.

Thereby, Vegard's law for solid solutions $(Al_xGa_{1-x}As_{1-y}P_y)_{1-z}Si_z$ can be written in general form as follows:

$$\begin{aligned} a_{(Al_xGa_{1-x}As_{1-y}P_y)_{1-z}Si_z} &= \left(\left(a_{AlP}x + a_{GaP}(1-x)\right)y \right. \\ &\quad \left. + \left(a_{AlAs}x + a_{GaAs}(1-x) + cx(1-x)\right)(1-y)\right) \\ &\quad \times (1-z) + a_{Si}z \\ &= \left(\left(5.4635x + 5.4508(1-x)\right)y \right. \\ &\quad \left. + \left(5.6533 + 0.00929\left(x - 0.143x^2\right)\right)(1-y)\right)(1-z) \\ &\quad + 5.431z. \end{aligned} \tag{2}$$

We used the lattice parameters values for binary compounds, presented in [15]: $a_{AlP} = 5.4635$ Å, $a_{GaP} = 5.4508$ Å, and $a_{Si} = 5.431$ Å.

Similarly, assuming a linear dependence of the Poisson's coefficient of atomic concentrations in solid solution, we can obtain the following relationship:

$$\begin{aligned} \nu_{(Al_xGa_{1-x}As_{1-y}P_y)_{1-z}Si_z} &= \left((0.300x + 0.306(1-x))y \right. \\ &\quad \left. + (0.325x + 0.312(1-x) \right. \\ &\quad \left. + 0.001245x(1-x))(1-y)\right) \\ &\quad \times (1-z) + 0.278z. \end{aligned} \tag{3}$$

Poisson's ratio for binary compounds was taken from [15] and was as follows: $\nu_{AlP} = 0.300$, $\nu_{AlAs} = 0.325$, $\nu_{GaP} = 0.306$, $\nu_{GaAs} = 0.312$, $\nu_{InP} = 0.359$, $\nu_{InAs} = 0.352$, and $\nu_{Si} = 0.278$.

Using relations (1)–(3) as well as the analysis of the reciprocal space maps for nodes (400) and (511) (see Table 3) enables us to calculate lattice parameters of five-component solid solutions $Al_xGa_yIn_{1-x-y}As_zP_{1-z}$ taking into account elastic stresses. Assuming that Vegard's law is obeyed for the obtained $(Al_xGa_{1-x}As_{1-y}P_y)_{1-z}Si_z$ solid solutions, we specified the concentrations of the elements (see Table 3) analyzing expressions (1)–(3) and calculation of the lattice parameters and data from microanalysis.

The strain coefficient of the alloy can be determined from XRD data as

$$\varepsilon = \frac{a_{(Al_xGa_{1-x}As_{1-y}P_y)_{1-z}Si_z} - a_{(GaAs)}}{a_{(GaAs)}}. \tag{4}$$

The results of calculations of the alloy allowing for elastic stresses are listed in Table 3. The calculated data show (see Table 3) that the implementation of phosphorus and silicon as an impurity of high concentrations can reduce the stress in epitaxial films.

The penetration depth of laser radiation and the effective depth of analysis with Raman scattering can be determined from the ratio $\lambda/2\pi k$, where k is extinction coefficient. For an argon laser with $\lambda = 532$ nm the analysis depth for AlGaAs is approximately 500 nm. It gives the right to say that using this laser wavelength for Raman scattering we obtain the information only from the layer of solid solution.

The selection rules derived from the analysis of the Raman scattering tensor [16] for crystals with diamond

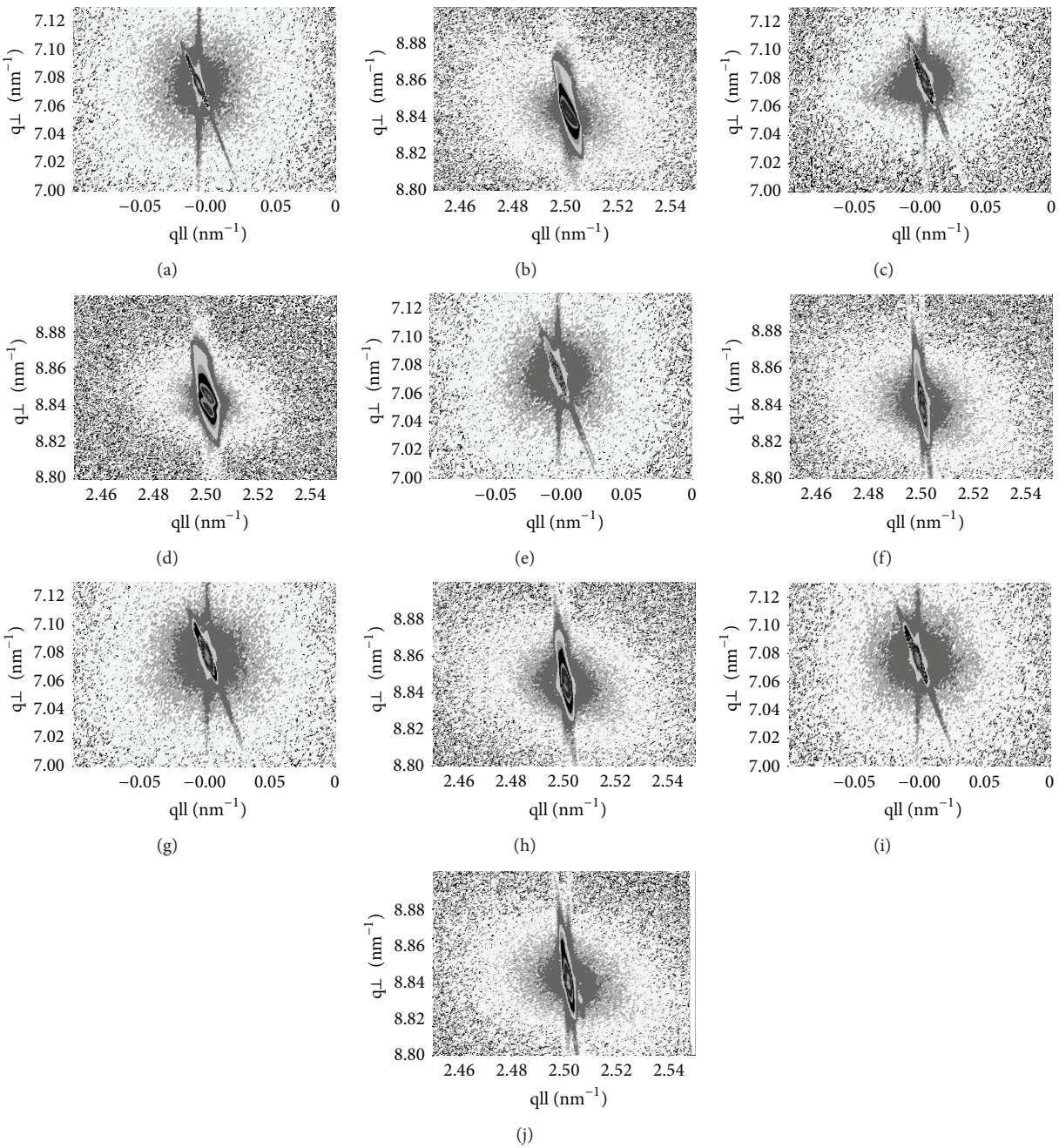

FIGURE 1: Reciprocal q-space maps for symmetric (400) and asymmetric (511) nods of $Al_xGa_{1-x}As_yP_{1-y}$:Si/GaAs (100) heterostructures. (a), (c), (e), (g), and (i) map of symmetric (400) nods. (b), (d), (f), (h), and (j) map of asymmetric (511) nods. (a) and (b) EM2350: GaAs; (c) and (d) EM2346: $Al_{0.26}Ga_{0.74}As$; (e) and (f) EM2343: $(Al_{0.33}Ga_{0.67}As_{0.995}P_{0.005})_{0.9997}Si_{0.0003}$; (g) and (h) EM2355: $(Al_{0.426}Ga_{0.574}As_{0.975}P_{0.025})_{0.999}Si_{0.001}$; (i) and (j) EM2356: $(Al_{0.43}Ga_{0.57}As_{0.977}P_{0.023})_{0.997}Si_{0.003}$.

structure with backscattering from the (100) surface allow one to observe only LO phonons, and the appearance of TO phonons is prohibited.

Figure 2 presents the spectra of Raman backscattering geometry for the samples to be analyzed, which are arranged for the convenience in the subgroups: Figure 2(a): spectrum of homoepitaxial structures, Figure 2(b): spectra of heterostructures based on ternary AlGaAs and four-component AlGaAsSi solid solutions, and Figure 2(c): spectra of heterostructures based on five-component AlGaAsPSi solid solutions.

As can be seen from the results, spectra of heterostructures include all of the major fluctuations specific to the type of heterostructures (vibration frequencies are presented in Table 4). Thus, from Figure 2 we can see that Raman spectrum of the structure of homoepitaxial GaAs/GaAs (100)

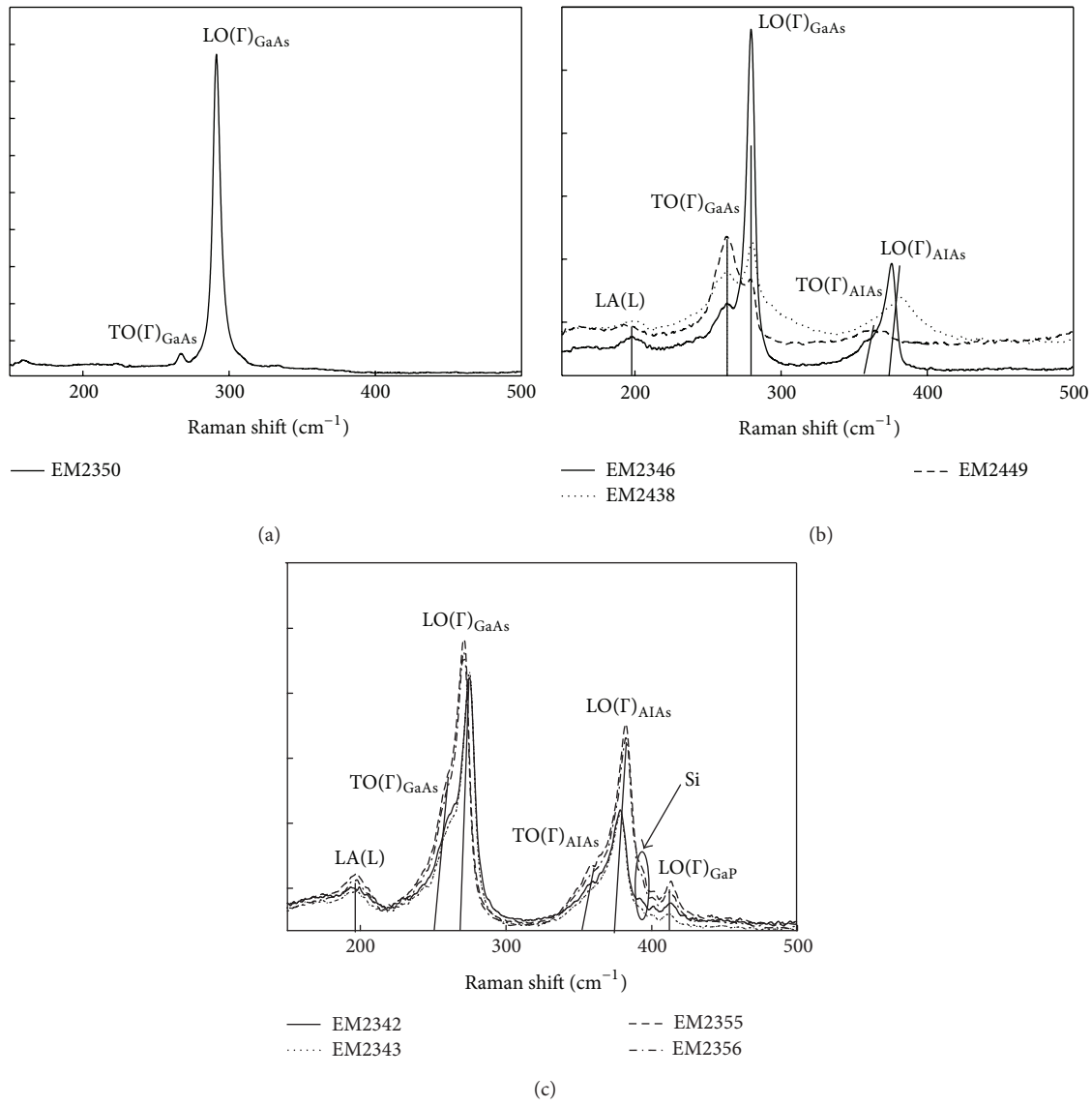

FIGURE 2: Raman backscattering spectra of the $Al_xGa_{1-x}As_yP_{1-y}$:Si/GaAs (100) heterostructures. (a) EM2350: GaAs; (b) EM2346: $Al_{0.26}Ga_{0.74}As$; EM2438: $Al_{0.22}Ga_{0.78}As$:Si (10^{-5}); EM2449: $(Al_{0.20}Ga_{0.80}As)_{0.999}Si_{0.001}$; (c) EM2342: $Al_{0.35}Ga_{0.65}As_{0.9999}P_{0.0001}$:Si ($10^{-5}$); EM2343: $Al_{0.35}Ga_{0.65}As_{0.9999}P_{0.0001}$:Si ($10^{-5}$); EM2355: $(Al_{0.426}Ga_{0.574}As_{0.975}P_{0.025})_{0.999}Si_{0.001}$; EM2356: $(Al_{0.43}Ga_{0.57}As_{0.977}P_{0.023})_{0.997}Si_{0.003}$.

(sample EM2350) contains high intensity longitudinal optical phonon LO(Γ) localized ~293 cm^{-1}. The experimental data, including the shape of the spectrum for the homoepitaxial sample, shows the dislocation-free mechanism of growth and excellent structural properties of the layer.

Raman spectra of heterostructures $Al_xGa_{1-x}As$:Si/GaAs (100) (samples EM2346, EM2438, and EM2449) contain longitudinal LO phonon modes of Ga-As and Al-As at (Γ), located in the range of ~267 cm^{-1} and ~380 cm^{-1}, respectively (see Figures 2(a) and 2(b)).

The main fluctuations presented in Raman backscattering spectra for heterostructures based on five-component $(Al_xGa_{1-x}As_{1-y}P_y)_{1-z}Si_z$ solid solutions are longitudinal (allowed) optical vibrations GaAs and AlAs and longitudinal mode GaP.

The experiment shows that in all the studied Raman backscattering spectra in addition to main vibration modes there are a number of additional modes. In the experimental Raman spectra of all heterostructures present transverse oscillation modes TO Ga-As and Al-As (forbidden by the selection rules), which is a consequence of disorientation solid solution epitaxial growth relative to the direction given by the substrate GaAs, having already disorientation relative to the direction (100).

It should be noted that in Raman spectra of EM2449 heterostructure, a solid solution doped with silicon with high concentration, the intensity of the transverse oscillation mode TO Ga-As is higher than the allowed longitudinal LO. It is most likely to be the result of disorders in crystal lattice symmetry in epitaxial layer due to its doping.

Table 3: Results of high-resolution XRD diffraction.

Sample	Composition, x	Lattice parameter a^{γ}, Å	Strain coefficient of the alloy, ε
EM2350 T = 800; flow = 0; carrier = 3.6×10^{16}	GaAs	5.6533	—
EM2346 T = 800; flow = 0; carrier = 3.1×10^{16}	$Al_{0.26}Ga_{0.74}As$	5.6555	0.00040
EM2438 T = 700; flow = 10; carrier = 3.4×10^{17}	$Al_{0.22}Ga_{0.78}As{:}Si(10^{-5})$	5.6553	0.00036
EM2449 T = 800; flow = 100; carrier = 6.5×10^{17}	$(Al_{0.20}Ga_{0.80}As)_{0.999}Si_{0.001}$	5.6549	0.00029
EM2342 T = 800; flow = 100; carrier = 7.85×10^{17}	$Al_{0.35}Ga_{0.65}As_{0.9999}P_{0.0001}{:}Si(10^{-5})$	5.6564	0.00056
EM2343 T = 800; flow = 200; carrier = 8.19×10^{17}	$(Al_{0.33}Ga_{0.67}As_{0.995}P_{0.005})_{0.9997}Si_{0.0003}$	5.6554	0.00038
EM2355 T = 800; flow = 200; carrier = 7.07×10^{17}	$(Al_{0.426}Ga_{0.574}As_{0.975}P_{0.025})_{0.999}Si_{0.001}$	5.6517	−0.00027
EM2356 T = 800; flow = 300; carrier = 4.56×10^{17}	$(Al_{0.43}Ga_{0.57}As_{0.977}P_{0.023})_{0.997}Si_{0.003}$	5.6518	−0.00026

The appearance of longitudinal acoustic phonons LA(L) is likely to be caused by a structural disorder, the replacement of atoms in metal and nonmetal sublattice [17].

Raman backscattering spectra of heterostructures with a high concentration of silicon in solid solution provide additional mode located at ~400 cm^{-1}. In accordance with the results of our previous studies [10, 11], the appearance of oscillations with frequencies close to 390 cm^{-1} is caused due to the fact that silicon atoms occupy space in the metal sublattice Si_{Ga} or Si_{Al}, that is, arise the Si–As oscillation (see Figure 2(c)). From these results it can be clearly seen that the intensity of additional mode depends on the initial flow of silicon source, silane and substrate holder temperature during growth. The greater the flow of silane and the lower the temperature are, the higher the concentration of silicon in the five-component solid solution is. This data agrees with the results of X-ray diffraction studies and the results of our previous studies devoted to $Al_xGa_{1-x}As{:}Si$ solid solutions.

Raman shift of the main active optical modes in spectra of heterostructures depends on the ratio of the atoms in the metal and nonmetal sublattice solid solution. The main frequencies of GaAs, AlAs, and GaP active modes are in agreement with the results of Raman backscattering research [18, 19] for ternary solid solutions $Al_xGa_{1-x}As$ and $Al_xGa_{1-x}P$.

The alterations in the composition and stoichiometry of solid solutions, including five-component layers in case of deep levels, complex defects, and complexes formation, are accompanied by rupture of the donor-crystal connection and donor atom displacement and changes in bond lengths in crystal lattice. All the above mentioned changes in solid solutions should emerge in the energy characteristics of the material and be reflected in photoluminescence spectra. Photoluminescence spectra of some of the samples shown in Figure 3 were obtained at room temperature in the 1.3–2.0 eV with excitation from argon laser with a wavelength

Table 4: Frequencies of active Raman mode in spectra of $Al_xGa_{1-x}As_yP_{1-y}$:Si heterostructures.

Sample	GaAs ω_{LO}/ω_{TO}, cm^{-1}	AlAs ω_{LO}/ω_{TO}, cm^{-1}	GaP ω_{LO}, cm^{-1}	$\omega_{LA(L)}$, cm^{-1}	Si-like, cm^{-1}
EM2350 GaAs T = 800; flow = 0; carrier = 3.6×10^{16}	291/267	—	—	—	—
EM2346 $Al_{0.26}Ga_{0.74}As$ T = 800; flow = 0; carrier = 3.1×10^{16}	279/263	376/358	—	197	—
EM2438 $Al_{0.22}Ga_{0.78}As$:Si(10^{-5}) T = 700; flow = 10; carrier = 3.4×10^{17}	278/262	360	—	197	—
EM2449 $(Al_{0.20}Ga_{0.80}As)_{0.999}Si_{0.001}$ T = 800; flow = 100; carrier = 6.5×10^{17}	279/263	379	—	196	—
EM2342 $Al_{0.35}Ga_{0.65}As_{0.9999}P_{0.0001}$:Si($10^{-5}$) T = 800; flow = 100; carrier = 7.85×10^{17}	281/263	373/359	413	198	—
EM2343 $(Al_{0.33}Ga_{0.67}As_{0.995}P_{0.005})_{0.9997}Si_{0.0003}$ T = 800; flow = 200; carrier = 8.19×10^{17}	276/263	377/360	411	196	392
EM2355 $(Al_{0.426}Ga_{0.574}As_{0.975}P_{0.025})_{0.999}Si_{0.001}$ T = 800; flow = 200; carrier = 7.07×10^{17}	274/263	378/356	413	196	393
EM2356 $(Al_{0.43}Ga_{0.57}As_{0.977}P_{0.023})_{0.997}Si_{0.003}$ T = 800; flow = 300; carrier = 4.56×10^{17}	271/263	382/356	412	197	392

of λ = 514.5 nm. As can be seen from the experimental data, the emission from the sample of homoepitaxial GaAs/GaAs (EM2350) is presented by a high-intensity peak at E_g = 1.43 eV, which is in excellent agreement with the published data. Photoluminescence spectra of the sample EM2346 belong to a conventional heterostructure $Al_{0.27}Ga_{0.73}As$/GaAs (100) and contain two emission bands with the energy in the range of $E_1 \sim 1.43$ eV and $E_2 = 1.81$ eV and that matches luminescence profile positions from the substrate and the solid solution. The greatest interest constitutes photoluminescence spectra of the samples EM2449, EM2342, and EM2355 that represent heterostructures based on the multicomponent solid solutions. Photoluminescence spectra of these images present high-intensity broad emission band located in area with energy $E \sim 1.3$–1.65 eV and have a number of peculiarities in the form of the shoulders. In addition to the spectra of heterostructures EM2449 and EM2342 there is a low intensity emission shifted towards the high-energy area. Energy emission profiles of photoluminescence spectra of heterostructures are presented in Table 5.

Based on the above linear interpolation for Vegard's law we can similarly use the relation between the band

Table 5: Photon energies corresponding to emission peaks in AlGaAsP:Si/GaAs (100) heterostructures.

	Experimental peak positions, eV						
	GaAs	Deep level				$(Al_xGa_{1-x}As_{1-y}P_y)_{1-z}Si_z$ solid solution, experiment	$(Al_xGa_{1-x}As_{1-y}P_y)_{1-z}Si_z$ solid solution, calculation from (5)
EM2350							
$T = 800$; flow = 0; carrier = 3.6×10^{16}	1.43	—	—	—	—		
EM2346							
$T = 800$; flow = 0; carrier = 3.1×10^{16}	1.43	—	—	—	—	1.81	1.80
EM2449							
$T = 800$; flow = 100; carrier = 6.5×10^{17}		1.39	1.45	—	—	1.74	1.72
EM2342							
$T = 800$; flow = 100; carrier = 7.85×10^{17}		1.395	1.475	1.53	1.58	1.935	1.91
EM2355							
$T = 800$; flow = 200; carrier = 7.07×10^{17}		1.395	1.475	1.53	1.58	—	2.00

gap and the atomic concentration for five-component $(Al_xGa_{1-x}As_{1-y}P_y)_{1-z}Si_z$ solid solutions. Consider

$$\begin{aligned} E_{g_{(Al_xGa_{1-x}As_{1-y}P_y)_{1-z}Si_z}} &= \big((2.261 + 0.219x)\, y \\ &\quad + \left(1.43 + 1.707x - 1.437x^2 + 1.31x^3\right) \\ &\quad \times (1 - y)\big)(1 - z) + 1.1z. \end{aligned} \tag{5}$$

The value of the band gap of Si $E_{g_{Si}} = 1.1$ eV was taken from [15].

Using relation (10) for $(Al_xGa_{1-x}As_{1-y}P_y)_{1-z}Si_z$ we can determine energy emissions $E_g(x, y, z)$ from the data obtained by photoluminescence spectra corresponding to the band gaps of solid solutions. The calculation shows that low intensity emission spectra of EM2449 and EM2342 samples are shifted to the high-energy areas and belong to multicomponent $(Al_xGa_{1-x}As_{1-y}P_y)_{1-z}Si_z$ heterostructures photoluminescence.

In our previous work [11] devoted to the research of highly doped heterostructures based on four-component $(Al_xGa_{1-x}As)_{1-y}Si_y$ solid solutions $(Al_xGa_{1-x}As)_{1-y}Si_y$, it was shown that the level of doping of silicon $n_{Si} \sim 0.1$ at.% may arise deeper levels, DX-centers, which are situated below the top of the conduction band at about 500 meV. We also managed to show that in photoluminescence spectra of heterostructures doped with high concentrations of silicon there is the main extinction of the exciton bands, which is connected with the formation of deep levels, where optical transitions are more favorable than the zone-to-zone transition (i.e., the emergence of the main exciton photoluminescence band) and also with the fact that the tetragonal compression in the solid solution $Al_xGa_{1-x}As$ should lead to a change in the band structure [20]. Proceeding from the experimental data received in our present work in the case of formation of multicomponent solid solutions with silicon $(Al_xGa_{1-x}As)_{1-y}Si_y$ and $(Al_xGa_{1-x}As_{1-y}P_y)_{1-z}Si_z$, grown on GaAs (100), we not only observe the formation of DX-centers, but also find a high degree of distortion in the epitaxial film in the direction of growth (tetragonal distortion), which changes the nature of the band structure and the lack of permits for solid solutions of optical transition zone-to-zone. Optical activation energy of the deep levels arising in multicomponent solid solutions $(Al_xGa_{1-x}As_{1-y}P_y)_{1-z}Si_z$ depends on the concentration of silicon dopant and according to our calculations remains in the range of 350–400 meV.

4. Results

Joint analysis of the experimental data obtained by high-resolution X-ray diffraction, elemental microanalysis, Hall measurements, Raman backscattering, photoluminescence spectroscopy, and calculations based on the experimental data allows some conclusions concerning the effect of doping with phosphorus and silicon on the structure and optical properties of the investigated heterostructures.

The implementation of phosphorus and silicon as an impurity of high concentrations transforms ternary $Al_xGa_{1-x}As$ solid solutions into five-component solid solutions $(Al_xGa_{1-x}As_{1-y}P_y)_{1-z}Si_z$. In this case, silicon behaves as

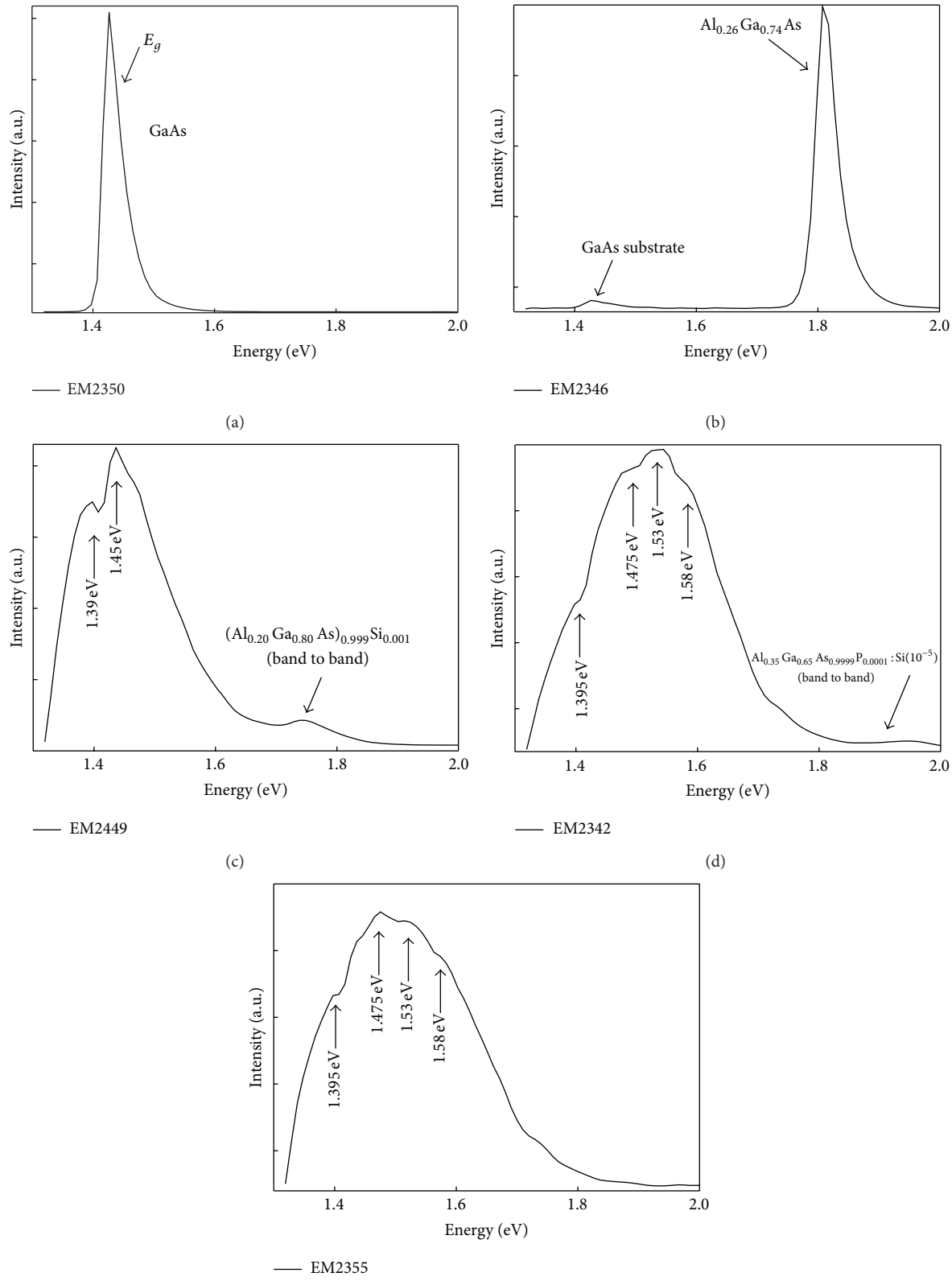

FIGURE 3: PL spectra of the $Al_xGa_{1-x}As_yP_{1-y}$:Si/GaAs (100) heterostructures. (a) EM2350: GaAs; (b) EM2346: $Al_{0.26}Ga_{0.74}As$; (c) EM2449: $(Al_{0.20}Ga_{0.80}As)_{0.999}Si_{0.001}$; (d) EM2343: $(Al_{0.33}Ga_{0.67}As_{0.995}P_{0.005})_{0.9997}Si_{0.0003}$; (e) EM2355: $(Al_{0.426}Ga_{0.574}As_{0.975}P_{0.025})_{0.999}Si_{0.001}$.

an amphoteric impurity and takes positions at regular nodes of metal and nonmetal sublattices.

The method of high-resolution X-ray diffraction showed that the obtained solid solutions are grown coherently on the single crystal substrate and have a good structural quality, which can be traced in the form of symmetric and asymmetric reflections in reciprocal space. Changes in the lattice parameters of five-component $(Al_xGa_{1-x}As_{1-y}P_y)_{1-z}Si_z$ solid solutions on the composition of the sample are subject to the imposed Vegard's law for this system and are well detected on the major permitted active modes in the Raman spectra.

In addition, the implementation of silicon in solid solution with a concentration of ~0.01 at.% leads to the formation of the structure with deep levels, DX-centers, the occurrence of which fundamentally affects the energy characteristics of the received materials.

The activation energy of deep levels, that is, the energy required to transfer an electron from the donor level in the conduction band according to our calculations, remains in the range of 350–400 meV.

Thus in photoluminescence spectra the extinction of the main emission bands takes place as a consequence of the DX-centers which form levels in the band gap, where optical transitions are more profitable. As a result, the conductivity of the investigated heterostructures is determined by the effects associated with recharging deep levels, as well as the residual effects of positive and negative photoconductivity, which makes these materials highly promising optical converters.

Conflict of Interests

The author declares that there is no conflict of interests regarding the publication of this paper.

Acknowledgments

The work was supported by Russian Federation Government Assignment for Higher Education Institutions (Projects no. 740, Task no. 3.130.2014/K). This work was partially supported by Notre Dame University Integrated Imaging Facility. The author acknowledges the Karlsruhe Nano Micro Facility (KNMF, http://www.kit.edu/knmf) of the Forschungszentrum Karlsruhe for providing the access to the equipment at their laboratories.

References

[1] Z. I. Alferov, "The history and future of semiconductor heterostructures," *Semiconductors*, vol. 32, no. 1, pp. 1–14, 1998.

[2] L. L. Chang and K. Ploog, Eds., *Molecular Beam Epitaxy and Heterostructures*, Springer, 1st edition, 1984.

[3] P. V. Seredin, A. V. Glotov, V. E. Ternovaya et al., "Spinodal decomposition of $Ga_xIn_{1-x}As_yP_{1-y}$ quaternary alloys," *Semiconductors*, vol. 45, no. 11, pp. 1433–1440, 2011.

[4] D. A. Vinokurov, V. A. Kapitonov, A. V. Lyutetskiy et al., "850-nm diode lasers based on AlGaAsP/GaAs heterostructures," *Semiconductors*, vol. 46, no. 10, pp. 1321–1325, 2012.

[5] A. A. Marmalyuk, M. A. Ladugin, I. V. Yarotskaya, V. A. Panarin, and G. T. Mikaelyan, "Laser diode bars based on strain-compensated AlGaPAs/GaAs heterostructures," *Quantum Electronics*, vol. 42, no. 1, pp. 15–17, 2012.

[6] D. T. Mathes, *Materials issues for VCSEL operation and reliability [Ph.D. thesis of Philosophy in Materials Science and Engineering]*, 2002.

[7] V. I. Borisov, V. A. Sablikov, I. V. Borisova, and A. I. Chmil', "Low-dimensional systems: charging of deep-level centers and negative persistent photoconductivity in modulation-doped AlGaAs/GaAs heterostructures," *Semiconductors*, vol. 33, no. 1, pp. 60–65, 1999.

[8] "3D projection full color multimedia display," WIPO Patent Application WO/2007/127269, 2007.

[9] US Patent Application 20100297608, "Systems and methods for CMOScompatible silicon nano-wire sensors with biochemical and cellular interface".

[10] P. V. Seredin, A. V. Glotov, E. P. Domashevskaya, I. N. Arsentyev, D. A. Vinokurov, and I. S. Tarasov, "Structural and optical investigations of AlxGa 1-xAs:Si/GaAs(1 0 0) MOCVD heterostructures," *Physica B: Condensed Matter*, vol. 405, no. 22, pp. 4607–4614, 2010.

[11] P. V. Seredin, A. V. Glotov, V. E. Ternovaya et al., "Effect of silicon on relaxation of the crystal lattice in MOCVD-hydride Al_xGa_{1-x} As:Si/GaAs(100) heterostructures," *Semiconductors*, vol. 45, no. 4, pp. 481–492, 2011.

[12] D. Zhou and B. F. Usher, "Deviation of the AlGaAs lattice constant from Vegard's law," *Journal of Physics D: Applied Physics*, vol. 34, no. 10, pp. 1461–1465, 2001.

[13] P. V. Seredin, A. V. Glotov, E. P. Domashevskaya, I. N. Arsentyev, D. A. Vinokurov, and I. S. Tarasov, "Structural features and surface morphology of AlxGa yIn1-x-yAszP1-z/GaAs(1 0 0) heterostructures," *Applied Surface Science*, vol. 267, pp. 181–184, 2013.

[14] P. V. Seredin, A. V. Glotov, E. P. Domashevskaya et al., "Structural and spectral features of MOCVD $Al_xGa_yIn_{1-x-y}As_zP_{1-z}$/GaAs (100) alloys," *Semiconductors*, vol. 46, no. 6, pp. 719–729, 2012.

[15] Y. A. Goldberg and N. M. Schmidt, *Handbook Series on Semiconductor Parameters*, vol. 2, World Scientific, London, UK, 1999, edited by M. Levinshtein, S. Rumyantsev and M. Shur.

[16] W. Hayes and R. Loudon, *Scattering of Light by Crystals*, John Wiley & Sons, New York, NY, USA, 1978.

[17] B. Jusserand and J. Sapriel, "Raman investigation of anharmonicity and disorder-induced effects in Ga1-xAlxAs epitaxial layers," *Physical Review B*, vol. 24, no. 12, pp. 7194–7205, 1981.

[18] D. J. Lockwood and Z. R. Wasilewski, "Optical phonons in $Al_xGa_{1-x}As$: raman spectroscopy," *Physical Review B: Condensed Matter and Materials Physics*, vol. 70, no. 15, Article ID 155202, 2004.

[19] D. P. Bour, J. R. Shealy, A. Ksendzov, and F. Pollak, "Optical investigation of organometallic vapor phase epitaxially grown $Al_xGa_{1-x}P$," *Journal of Applied Physics*, vol. 64, no. 11, pp. 6456–6459, 1988.

[20] S. Laref, S. Meçabih, B. Abbar, B. Bouhafs, and A. Laref, "First-principle calculations of electronic and positronic properties of AlGaAs2," *Physica B: Condensed Matter*, vol. 396, no. 1-2, pp. 169–176, 2007.